International Journal of Pharmaceutics 647 (2023) 123489

Contents lists available at ScienceDirect

International Journal of Pharmaceutics

journal homepage: www.elsevier.com/locate/ijpharm

Microfluidic manufacturing of tioconazole loaded keratin nanocarriers: Development and optimization by design of experiments

Shiva Khorshid [a], Rosita Goffi [a], Giorgia Maurizii [a], Serena Benedetti [a], Giovanna Sotgiu [b,c,*], Roberto Zamboni [b,c], Sara Buoso [c], Roberta Galuppi [d], Talita Bordoni [d], Mattia Tiboni [a], Annalisa Aluigi [a,c,*], Luca Casettari [a]

[a] Department of Biomolecular Sciences, University of Urbino Carlo Bo, Piazza del Rinascimento, 6, 61029 Urbino (PU), Italy
[b] Institute of Organic Synthesis and Photoreactivity – Italian National Research Council, Via P. Gobetti, 101, Bologna, 40129, Italy
[c] Kerline srl, Via Piero Gobetti 101, Bologna, 40129, Italy
[d] Department of Veterinary Medical Sciences, University of Bologna, Ozzano dell'Emilia, Bologna, 40064, Italy

ARTICLE INFO

Keywords:
Keratin
Design of Experiment
Nanomedicine
Microfluidics
Mycosis
Antifungal therapy

ABSTRACT

Fungal infections of the skin, nails, and hair are a common health concern affecting a significant proportion of the population worldwide. The current treatment options include topical and systematic agents which have low permeability and prolonged treatment period, respectively. Consequently, there is a growing need for a permeable, effective, and safe treatment. Keratin nanoparticles are a promising nanoformulation that can improve antifungal agent penetration, providing sustainable targeted drug delivery. In this study, keratin nanoparticles were prepared using a custom-made 3D-printed microfluidic chip and the manufacturing process was optimized using the design of experiments (DoE) approach. The total flow rate (TFR), flow rate ratio (FRR), and keratin concentration were found to be the most influential factors of the size and polydispersity index (PDI) of the nanoparticles. The crosslinking procedure by means of tannic acid as safe and biocompatible compound was also optimized. Keratin nanoparticles loaded with a different amount of tioconazole showed a size lower than 200 nm, a PDI lower than 0.2 and an encapsulation efficiency of 91 ± 1.9 %. Due to their sustained drug release, the formulations showed acceptable *in vitro* biocompatibility. Furthermore, a significant inhibitory effect compared to the free drug against *Microsporum canis*.

1. Introduction

Cutaneous mycoses affect nearly 25 % of the human population worldwide (Havlickova et al., 2008). These infections are generated mainly by dermatophytes, which produce a broad spectrum of proteolytic enzymes which are able to degrade the natural keratin of skin, hair, and nails (Mercer and Stewart, 2019). The initial stage of biodegradation is the breaking of disulphide bonds present in the keratin by sulphitolysis: reaction which seems to facilitate the extracellular biodegradation of keratin by the dermatophytes' extensive array of endo- and exoproteases (Mercer and Stewart, 2019).

Due to the limited availability at the site of action of the antifungal drugs, the prescribed doses for oral therapies escalated, or the dosing frequency increased. This results in an increase in associated side effects such as drug interactions and hepato-toxicity (Rocha et al., 2017). Topical therapy is the most desirable treatment route due to limited side effects and drug interactions as well as better patient compliance. The limitation of the use of topical antifungal is their low permeability, especially through the skin or nail plates (Rocha et al., 2017). One of the approaches used to overcome this drawback relies on the use of nanoparticles encapsulating the antifungal, which is released slowly over a prolonged period. The encapsulation of antimicrobials into

Abbreviations: DoE, design of experiment; TFR, total flow rate; FRR, flow rate ratio; BDD, box-behnken design; CAD, computer-aided design; FDM, fused deposition modeling; Z-chip, zigzag- chip; TA, tannic acid; GA, glutaraldehyde; TCZ, tioconazole; KNPs, keratin nanoparticles; TCZ-KNPs, tioconazole loaded keratin nanoparticle; *M. canis*, *Microsporum canis*; PDI, polydispersity index; DLS, dynamic light scattering; FTIR, fourier-transformed infrared spectroscopy; DMEM, dulbecco's modified eagle medium; WST-8, water-soluble tetrazolium 8; SRB, sulforhodamine B; MD, microdilution method; MIC, minimum inhibitory concentration; MLC, minimum lethal concentration.

* Corresponding authors.
E-mail addresses: giovanna.sotgiu@isof.cnr.it (G. Sotgiu), Annalisa.aluigi@uniurb.it (A. Aluigi).

https://doi.org/10.1016/j.ijpharm.2023.123489
Received 14 July 2023; Received in revised form 14 September 2023; Accepted 4 October 2023
Available online 5 October 2023

nanoparticles allows to reduce the drug toxicity and improves drug targeting (Amaral and Felipe, 2013; Dube et al., 2014). Different kinds of nanoparticles have been proposed for the delivery of antifungal drugs, including polymeric nanoparticles, solid lipid nanoparticles, liposomes, and magnetic nanoparticles (Souza and Amaral, 2017).

A particularly interesting material for vehiculating antifungal drugs is keratin extracted from mammalian hair such as wool and/or hair, due to its biodegradability, biocompatibility, but above all, for its high affinity towards keratinaceous appendices attacked by dermatophytes (Costa et al., 2022). In the last decade, there has been a growing interest in the use of keratin for the preparation of nanoparticles useful for the controlled delivery of drugs (Giannelli et al., 2022). The methods commonly used for the preparation of keratin nanoparticles loaded with active ingredients include desolvation, electrospray, self-assembling, ionic gelation, microemulsion and salting out (Giannelli et al., 2022). Although they are widely used methods for nanoparticles manufacturing, they lack in reproducibility especially when scaled up at pre-industrial or industrial level.

To overcome these drawbacks, the microfluidic-assisted desolvation processes are getting more attention, since they allow the formation of nanoparticles with controlled and reproducible size (Luo et al., 2011). In microfluidics, the formation of nanoparticles occurs under laminar flow, mixing the polymer phase with the desolvating phase in microchannels. Practically, by controlling the flow rate ratio (FRR) between the two phases, the total flow rate (TFR) of the two streams, and the concentration of the carrier, it is possible to tune the final size and distribution of resulting nanoparticles (Valencia et al., 2012) and batch-to-batch reproducibility (Ma et al., 2022; Forigua et al., 2021). Compared with traditional nanoparticle preparation methods, microfluidics shows several advantages such as providing better process control, continuous flow process, small footprint of the production apparatus, high production efficiency, and easy process scale-up (Khorshid et al., 2022a; Tiboni et al., 2021).

Moreover, as the majority of the protein carriers, KNPs tend to rapidly dissolve in physiological buffers; therefore, the use of of cross-linking agents seems to be inevitable to enhance their properties and attain a controlled drug delivery (Aluigi et al., 2016).

Based on biopolymer's application, type, and nature, the crosslinking method could be tailored by either physical (*e.g.,* UV irradiation, gamma radiation, and dehydrothermal treatment) or chemical crosslinking agents (*e.g.,* Glutaraldehyde, PEG, Genipin, etc). Despite the low toxicity of the physical crosslinking method, chemical crosslinkers are more used due to their higher efficiency. Since most chemical crosslinking agents are mostly toxic (*e.g.*, Glutaraldehyde) or expensive (*e.g.*, Genipin) (Chun et al., 2018), using a crosslinking agent to provide high efficiency and biocompatibility at a low price seems to be highly demanded.

Tannic Acid (TA) is an FDA-approved (Li et al., 2018), plant-derived polyphenol (Ahmadian et al., 2021) which is considered a safe biocompatible compound (Ninan et al., 2016), with anti-inflammatory, antimicrobial, antioxidant (Ahmadian et al., 2021; Gülçin et al., 2010; Ninan et al., 2016) and antiviral effects (Ninan et al., 2016). Moreover, TA is a cost-effective biomolecule (Ninan et al., 2016) with the ability to form different molecular interactions, with various polymers and molecules, including ionic, hydrophobic, and hydrogen binding (Sarker et al., 2022).

Within this scenario, a microfluidic-assisted desolvation approach has been here considered for the first time, for obtaining keratin nanoparticles (KNPs) loaded with tioconazole as antifungal agent (KNPs-TCZ), useful for the mycosis treatment.

Tioconazole is a broad-spectrum antifungal agent indicated for the topical treatment of onychomycosis (at a concentration of 28 %) and dermatomycoses (at a concentration of 1 %) (Clissold and Heel, 1986).

In order to optimize an efficient and scalable manufacturing process of keratin nanoparticles, a Design of Experiment (DoE) approach has been implemented. In particular, the Box-Behnken design (BDD) and the Response Surface Methodology (RSM) were the tools used to define the "design space" which correlates the process parameters as well as their interactions with the nanoparticles properties (MONTGOMERY, 2012)

Afterwards, the crosslinking process of keratin nanoparticles with tannic acid was optimized and compared with the one using GA in order to establish its efficacy.

Finally, the effectiveness of the tioconazole-loaded keratin nanoparticles crosslinked with TA, was assessed through *in vitro* models, also on a hair substrate.

2. Materials and methods

2.1. Material

Keratin was kindly provided by Kerline srl (Bologna, Italy). Tioconazole (TCZ, whose water solubility in ethanol is 0.0165 mg/mL and solubility in PBS:ethanol 1:3 is 0.25 mg/mL) and all the other chemicals were obtained from Merck (Milan, Italy). All solvents used were analytical grade.

2.2. Microfluidic assembly of keratin nanoparticles

KNPs were fabricated through microfluidic assisted desolvation method, using an in-house 3D-printed zig-zag microfluidic chip (Z-chip) fabricated using polypropylene (PP) with the fused deposition modelling (FDM) 3D printing technique (Tiboni et al., 2021). Briefly, the Z-chip is made of two inlets combined with a T junction into the main channel presenting a zigzag structure along its length. The total length of the main channel is 60 mm, its square section is of 1 mm; while the zigzag structure has a height of 500 μm (Tiboni et al., 2021).

Keratin was dissolved in water at a desired concentration and the nanoparticles were produced by mixing the aqueous phase with the ethanol (organic phase) at a specific ratio using the microfluidic system. The solutions were charged into polypropylene syringes, placed in two different pumps and the mixing was carried out in the previously described 3D-printed microfluidic chip. Several conditions for TFR, FRR, and keratin concentrations were set according to the design test (Table 1). Before collecting each run's formulation, clean run for a few seconds was mandatory due to the trapped air and dead volume.

The cross-linking process was carried out on the optimized formulation obtained using a keratin concentration of 10 % w/V, TFR 14 mL/min, and FRR 1:1. Both TA and GA were considered as the crosslinking agents. For the crosslinking process of KNPs with TA, different aliquots of an aqueous TA solution 10 % w/V concentrated, were added to the KNPs suspension in order to have 0.5, 0.7, 0.9 μL of TA solution (10 %w/V) per mg of KNP. The mixtures were maintained under stirring at 200 rpm for 4, 8, and 24 h at room temperature. Thereafter, 1 mL of the cross-linked formulations were placed in a dialysis bag (MW cut off 12 k-14 k Da, Spectra/Por™, Spectrum Labs, USA), immersed into 50 mL of distilled water to remove the ethanol and free cross-linkers through 24 h of dialysis at 100 rpm and room temperature. In order to cross-link the KNPs with GA, 0.4 μL per mg of KNPs of a GA aqueous solution 25 % w/V concentrated, were added to the fresh KNPs, and the mixture was maintained under stirring for 24 h. The rest of the process is as mentioned for TA. The crosslinking with TA was studied by attenuated total reflectance Fourier-transformed infrared spectroscopy ATR-FTIR (Perkin Elmer, MA, USA), operating in the 400–4000 cm^{-1} range at a resolution of 4 cm^{-1}.

Table 1
Independent variables: factors and their levels for the Box–Behnken design.

Factors	**Levels**		
Input variables	Low	Medium	High
Keratin Concentration (% w/V) -X_1	0.5	1	1.5
TFR (mL/min) -X_2	14	22	30
FRR -X_3	1	2.5	4

To obtain KNPs loaded with 5 %, 10 %, 15 %, 20 %, and 30 % w/w of tioconazole concerning keratin weight, the desired amount of tioconazole was solved in the ethanolic phase and mixed through the microfluidic device with the aqueous phase, as previously described, by applying the optimized parameters for the KNPs manufacturing process, followed by optimized crosslinking procedure (Fig. 1).

2.3. Keratin nanoparticles characterization

To investigate the physical properties of the formulation, the average particle size (Z- average) and polydispersity index (PDI) were determined using Malvern Zetasizer Nano S instrument (Malvern Instrument Ltd, UK). Formulations were diluted 1:10 with distilled water before measuring the sample with DLS. Moreover, to investigate the effect of cryoprotection during the freeze-drying process, different concentrations of the cryoprotectant trehalose (1 %, 5 %, 10 %, 20 % w/V) were dissolved in 500 µL of KNPs solution (0.5 % w/V) loaded with 30 % w/w of TCZ, cross-linked with TA and purified by dialysis as described before. These solutions were freeze-dried and the obtained powders were resuspended with the same amount of water (500 µL) and the rehydrated products were characterized in terms of their average particle size and polydispersity index by dynamic light scattering (DLS). To evaluate stability, a suspension of TCZ-loaded KNPs (5 mg/mL) was stored at 4 °C for 4 weeks and characterized in terms of particle size and PDI.

The morphology of nanoparticles was investigated by scanning electron microscope (SEM) using a Zeiss EVO LS 10 instrument equipped with a LaB6 source, by using an acceleration voltage of 5 kV and a working distance of 6.1 nm. The sample for SEM analysis was prepared by deposition of nanoparticles solution (0.1 mg/mL) on a silice slide, followed by gold spattering for 4 min. The interaction between keratin and TA was assessed on freeze-dried KNPs by the attenuated total FTIR (ATR-FTIR, Spectrum Two FT-IR spectrometer with ATR accessory, Perkin Elmer, MA, USA), in the wavenumbers range of 500–4000 cm^{-1}.

2.4. Design of experiments (DoE)

The DoE approach was used to individuate the parameters of microfluidic process affecting the characteristics of KNPs. In particular, the Box-Behnken statistical design (BDD) was implemented to evaluate the effects of the three independent variables *i.e.,* keratin concentration (X_1), TFR (X_2), and FRR (X_3) on the size and PDI of nanoparticles. For each independent variable, low, medium, and high levels were defined (Table 1) based on preliminary experimental work (data not shown). A total of 15 experiments were planned, combining the minimum, maximum, and intermediate independent variable values, according to the BDD design (Table S1). Matlab (Math Work, USA) was used to generate the BDD table of experiments. Each run was made in triplicate and the nanoparticle's size and PDI were measured as previously described. A multiple regression model was performed to establish relationships between the selected independent and dependent variables.

2.5. Quantitative determination of TCZ by HPLC

TCZ content, encapsulation efficiency, and drug release were evaluated by high-performance liquid chromatography (HPLC Agilent 1260 Infinity II, Agilent, USA) using an isocratic mixture of 0.5 % formic acid in water and 0.5 % formic acid in acetonitrile (ratio 50:50) as mobile phase, with a flow rate of 1 mL/min in an Agilent Poroshell 120 EC-C18, 100 × 4.6 mm, 2.7 µm column (Agilent, USA). The injection volume was 20 µL and the detection signal was recorded at 219 nm, keeping the analysis system at room temperature.

2.6. Encapsulation efficiency and loading content studies

Encapsulation efficiency (EE) and Loading Content (LC) of TCZ was calculated by indirect method and only for the sample prepared by using the 30 % w/w of TCZ versus KNPs. To this end, the prepared TCZ-KNPs suspension was diluted 1:5. Afterward, 1 mL of the diluted suspension was placed in dialysis tubing cellulose membrane (MW cut off 12-14 k

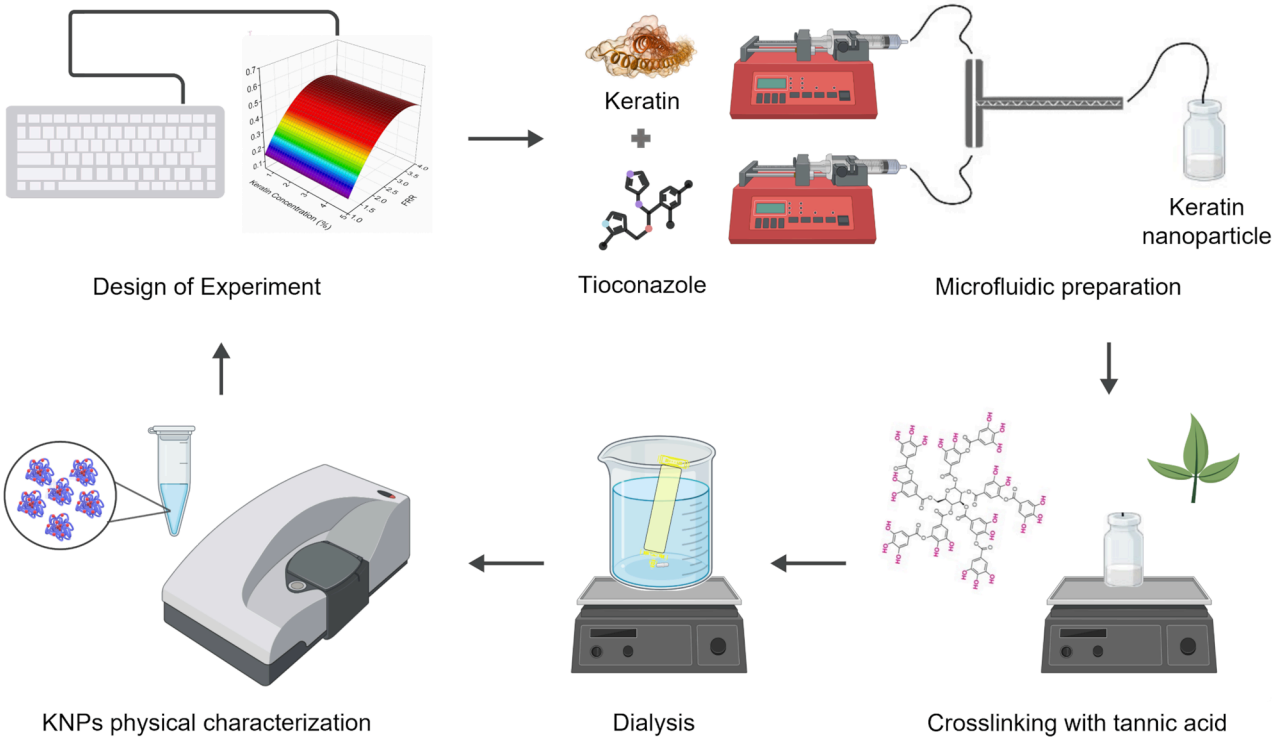

Fig. 1. Microfluidic assembly of KNPs using Design of Experiment implemented to accelerate the identification of the most significant variable and crosslinking and physical characterization. Image by biorender.com and freepik.

Da, Spectra/Por™, Spectrum Labs, USA), and dialyzed against 100 mL of deionized water under moderate stirring (100 rpm), ensuring sink conditions. The unloaded TCZ was assessed by HPLC. The encapsulation efficiency was defined as the ratio of the actual and original amount of TCZ encapsulated in NPs (Eq.1):

$$EE(\%) = \frac{total\ amount\ of\ TCZ(mg) - amount\ of\ TCZ\ in\ external\ water(mg)}{totalamount\ of\ TCZ(mg)} \times 100 \quad (1)$$

The loading content was defined as the ratio between the amount of the effectively loaded TCZ and the weight of the TCZ loaded KNPs (Eq.2)

$$LC(\%) = \frac{amount\ of\ loaded\ TCZ\ (mg)}{weight\ of\ the\ TCZ\ loaded\ KNPs\ (mg)} \times 100 \quad (2)$$

2.7. Drug release

The *in vitro* release of TCZ from TCZ-KNPs was evaluated in a release medium composed of 70 % of PBS and 30 % of EtOH, at 37 °C. For this study, the KNPs-TCZ suspension dialyzed as previously described (3 mL) was placed into a dialysis bag (MWCO = 12 to 14 kDa, Sigma Aldrich Corporation, USA) and put in contact with 50 mL of release medium to ensure that sink conditions were maintained, in sealed glass bottles. The bottles were maintained at 37 °C, under moderate and constant stirring (100 rpm) for 24 h. At pre-determined time intervals (5, 10, 15, 30, 45, 60,90 min, and 2, 4, 6, 8, and 24 h), 1 mL of the external medium was collected and replaced with the same volume of fresh medium. The amount of TCZ released from the KNPs was measured with HPLC, under the conditions described above.

2.8. Cell compatibility assay

The human keratinocyte cell line HaCaT (CLS-Cell Lines Service GmbH, Eppelheim, Germany) was maintained in Dulbecco's modified eagle medium (DMEM) supplemented with 10 % fetal bovine serum, 1 % L-glutamine, and 1 % penicillin/streptomycin 100 U/mL. To test KNPs' cytocompatibility, HaCaT cells (5×10^3/well) were seeded in 96-well plates and treated for 24 h with increasing concentrations of KNPs (up to 1 mg/mL). After incubation, cell viability was evaluated by both water-soluble tetrazolium (WST)-8 and sulforhodamine B (SRB) assays, which estimate cell metabolic activity and cell protein content, respectively, as previously described (Tiboni et al., 2020). Color development was monitored in a multi-well plate reader (ThermoFisher Scientific, Milan, Italy) and data were expressed as cell viability (%) versus untreated control cells.

2.9. In vitro microbiological studies

Different screening tests were conducted on three field strains (named 139, 80, and 59) of the dermatophyte *Microsporum canis*, isolated from skins of different cats, with and without lesions. The samples were collected by brushing technique for diagnostic purpose on owned cats. The strains were maintained through serial transplants on Sabouraud Dextrose Agar (BD) with 0.05 % of chloramphenicol (Sigma-Aldrich, Milan, Italy) (SAB-CAF) plates. For each strain the inoculum was obtained by covering a 14 days-old SAB-CAF culture dish with 10 mL of sterile RPMI 1640 medium (Sigma-Aldrich, Milan, Italy); subsequently, the colony was gently scraped with the tip of a pipette. The resulting mixture of conidia and hyphal fragments was drawn and transferred into tube containing five sterile glass balls, vortexed for 2–3 min, and kept at room temperature for 10 min (Singh et al., 2007). The supernatant suspension was transferred to another tube and the optical density was visually adjusted to level 2 of the McFarland scale (Galuppi et al., 2010).

The tested products were: a suspension of KNPs (3.4 mg/mL), a suspension of TCZ-KNPs (3.2 mg/mL, containing about 27 % of TCZ), and free TCZ (Merck, Milan, Italy) solubilized in ethanol. The products were diluted in RPMI 1640 medium at twice the highest tested concentrations of the antifungal drug (2 mg/mL for TCZ-KNPs and KNPS; 0.544 mg/mL for TCZ) and sterilized by autoclave at 121 °C for 15 min.

2.9.1. Microdilution method (MD)

For the MD test, a 96-well microtiter plate (Thermo Fisher, Milan, Italy) was used. Each well in columns 1 to 10 were filled with 100 μL of ten different 2-fold dilutions of each product, while columns 11 and 12 with 100 μL of sterile RPMI 1640 medium only. One-hundred microliters of inoculum were added to each well in columns 1 to 10. The growth control wells (column 12), which contained 100 μL of sterile drug-free medium, were also inoculated with 100 μL of the same inoculum suspension. Column 11 of the microdilution plate is filled with further 100 μL of RPMI 1640 as a sterility control for medium.

The final concentration of the tested products was two-fold diluted from 1 to 0.00125 mg/mL for both KNPs and TCZ-KNPs and from 0.272 to 0.00053 mg/mL for TCZ (corresponding to the TCZ content in TCZ-KNPs) (Table 2). Each strain was tested in triplicate. The plates were incubated at 26 °C for 11 days. The minimum inhibitory concentration (MIC) was defined as the lowest concentration that produced 100 % inhibition of growth. 10 μL from each not growing or not well growing well were inoculated on SAB-CAF plates, incubated at 26 °C, and observed for growth. The minimum lethal concentration (MLC) was defined as the lowest concentration inhibiting any further growth of the mycelium after 10 days of incubation.

2.9.2. Diffusion method on agar

For each strain tested, three SAB-CAF medium Petri dishes were inoculated by dipping a sterile cotton swab into the inoculum suspensions and streaming the swab in four directions over the entire agar surface. The dishes were allowed to dry for 5 min, then three 10 μL drops of the different products at twice the maximum concentration tested (2 mg/mL for TCZ-KNPs and KNPS; 0.544 mg/mL for TCZ) were dropped off onto the surface of each plate and allowed to dry. Inhibition zone diameters were periodically observed up to 11 days of incubation at 26 °C.

2.9.3. In vitro inhibition of M. Canis

Short strands of human hair were sterilized by autoclaving (121 °C for 15 min) and distributed in three petri dishes and 25 mL of sterile deionized water and 3 drops of sterile yeast extract (10 %) were added (Kurtzman et al., 2011). The plates were inoculated with 300 μL of each suspension of *M. canis* and observed after 4 weeks for mycelium growth and the presence of perforation in the hair (Figure S1). Subsequently, twenty-four-well plates were used. One well row was used for each strain: the wells of the columns from 1 to 5 were filled with 1 mL of two-fold dilution in RPMI 1640 medium of the products tested while the sixth well was used as control and contained only 1 mL of RPMI 1640 medium. The final concentrations of the products tested were from 1 to

Table 2
Concentration used of the tested products. The concentrations of TCZ alone be equivalent to the tioconazole content in TCZ-KNPs.

n. Dilution	TCZ-KNPs and KNPs (mg/mL)	TCZ (mg/mL)
1	1	0.272
2	0.5	0.136
3	0.25	0.068
4	0.125	0.034
5	0.0625	0.017
6	0.03125	0.0085
7	0.01562	0.00425
8	0.00781	0.00212
9	0.00390	0.00106
10	0.00195	0.00053

0.0626 mg/mL for both KNPs and TCZ-KNPs and from 0.272 to 0.017 mg/mL for free TCZ (corresponding to dilution from 1 to 5 of Table 2). Groups of hairs colonized by each strain were sterilely placed in each well. The plates were incubated at 26 °C. After 18, 24, 48, 120, and 288 h of contact, a few hairs from each well were passed onto plates of SAB-CAF and incubated at 26 °C and observed periodically for growth for up to 20 days to determine the death of *M. canis* at different concentrations and at different times of contact.

2.10. Statistical analysis

All data were expressed as the mean ± standard deviation (SD) based on at least three tests. The analysis of variance (ANOVA) with a statistically significant level of 5 % (p-value < 0.05) was used to define the regression mathematical models.

Moreover, the multiple correlation coefficient (R^2), the adjusted multiple correlation coefficient (adj-R^2) and the predictive (R^2-pred) were considered to validate the regression models. Having R^2 value closer to 1 indicates a perfect fit; however, R^2 generally increases by adding new terms in the regression model, even if they are not significant. The adj-R^2 is an adjustment of R^2 for the number of terms in the regression model and it increases if the new term improves the regression model; while it decreases when the term does not improve the regression model. Finally, the predictive R^2 (R^2-pred) was considered to evaluate how efficiently the regression model predicts output responses for new observations (Rebollo et al., 2022). One-way ANOVA with a significance level of 5 % was also performed to discuss results of the crosslinking and the cytotoxicity tests. All the statistical analysis were carried out using MATLAB (MathWork, USA) and Origin software (Origin Pro 2021b).

3. Results and discussion

3.1. Study of the correlations between process parameters and nanoparticles size and PDI

In order to develop a robust manufacturing process of KNPs by means of microfluidic assisted desolvation process, the BDD - DoE approach was implemented to study the effects of input variables (process parameters) and their interactions on the output (size and PDI) through a significantly reduced number of targeted experiments listed in Table S1 (Hashiba et al., 2020; Rebollo et al., 2022; Tao et al., 2021; Whiteley et al., 2021). Based on the previous microfluidic studies (Khorshid et al., 2022b; Rebollo et al., 2022; Zhang et al., 2020), FRR, TFR, and keratin concentration were selected as the input variables. The response surface methodology (RSM) is here used for modelling the process where the output variables are influenced by the selected input variables (Toms et al., 2017). The main outcome is the definition of the design space (DS), that is the region of the experimental domain input data and output data are correlated by means of a multivariable polynomial relationship. The advantage to define the DS relies on the possibility to predict the product's properties obtained with specific process parameters within the experimental domain.

In Fig. 2, the mean values and standard deviations of the nanoparticles obtained for each run are shown. These values were fitted using the quadratic polynomial model at three variables, described in equation (3) (Eq.3):

$$Y_0 = \beta_0 + \sum_{i=1}^{3} \beta_i X_i + \sum_{ij=1}^{3} \beta_{ij} X_i X_j + \sum_{i=1}^{3} \beta_{ii} X_i^2 \quad (3)$$

The significant parameters and related coefficients were selected based on the *p-values* obtained through the ANOVA test; particularly, the coefficient regression term is included in regression model if the *p-value* is lower than 0.05.

3.1.1. Effects of the process parameters on size

The experimental values of the KNPs size were fitted with the equation (3) and the obtained regression coefficients are listed in Table 3. As can be noted, all the equation terms containing the independent variable X_2, are not significant (*p-value* > *0.05*). A conclusion drawn from the results is that within the specified range of values, the size of the nanoparticles is not affected by TFR. By selecting the

Table 3
ANOVA parameters and validation of the Design Space.

Parameters	**Size (nm)** *p-value*		**PDI** *p-value*	-
X_1-Keratin Conc	0,0085	significant	0.9289	–
X_2-TFR	0,5535		0.6891	–
X_3-FRR	0,0021	significant	0.0096	significant
X_1X_2	0,0554		0.9392	–
X_1X_3	0,0026	significant	0.6375	–
X_2X_3	0,5594		0.7342	–
X_1^2	0,0089	significant	0.4184	–
X_2^2	0,2299		0.3112	–
X_3^2	0,0003	significant	0.021	significant
	Equation (3)	**Equation (4)**	**Equation (3)**	**Equation (5)**
R^2	0.9576	0.8825	0.8889	0.8267
Adj-R^2	0.8811	0.8172	0.6889	0.7978
Pred-R^2	0.2177	0.6190	−0.8961	0.7391
Validation	Experimental value	Predicted value	Experimental Value	Predicted value
Selected conditions: X_1 = 1 %; X_2 = 14 mL/min; X_3 = 1	112 ± 7 (nm)	111 ± 18 (nm)	0.10 ± 0.02	0.14 ± 0.07

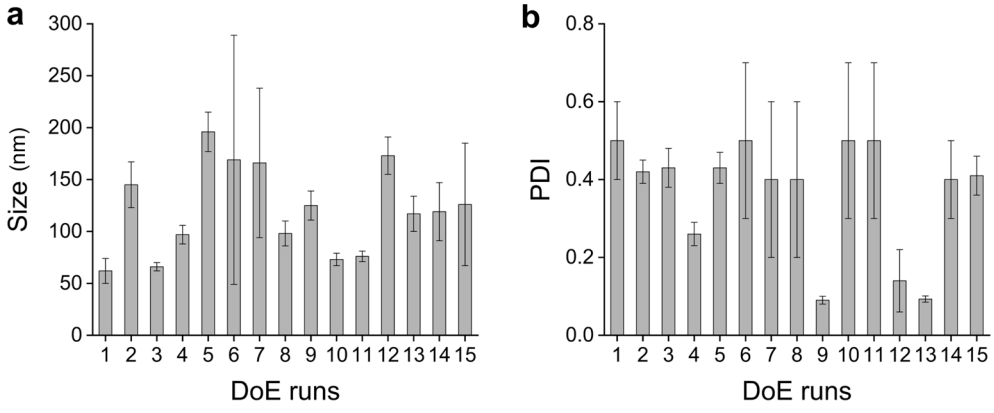

Fig. 2. Particle size (a) and PDI (b) results of all experiments performed.

significant coefficients with a *p-value* < *0.05*, the fitting equation can be simplified as follow (equation (4):

$$SIZE(nm) = 206.73 - 121.92X_1 - 62.74X_3 - 78.27X_1X_3 + 134.18X_1^2 + 33.23X_3^2 \quad (4)$$

By comparing the ANOVA parameters related to equations (3) and (4) (Table 2) for size, it can be observed that both equations have a *p-value* < *0.05*. Moreover, the adj-R^2, the adjustable R^2 associated with both equations (3) and (4) are in reasonable agreement; while the predicted R^2 is higher for equation (4) than for equation (3), thereby indicating that equation (4) can be used to navigate the design space (Fig. 3a).

3.1.2. Effects of the process parameters on PDI

The experimental values of PDI were first fitted with equation (3). Based on the *p-values* shown in Table 2, it appears that only the FRR significantly affects the PDI. Therefore, the equation can be simplified as follow (equation (5):

$$PDI = -0.2392 + 0.4553X_3 - 0.0706X_3^2 \quad (5)$$

As indicated by the ANOVA parameters listed in Table 2, equation (5) can be used to navigate the design space (Fig. 3b) since it shows a significant p-value lower than 0.0001, an adjusted-R^2, and a R^2-pred, higher than those obtained with equation (3).

3.1.3. Identification of main factors influencing size and size distribution

Based on the designed experiment results, it was determined that both the FRR and keratin concentration had a significant impact on the particle size. Regarding PDI, analysis identified FRR as the only significant factor. Through screening analysis, optimal values of FRR of 1 and keratin concentration at 1 % w/V were determined. Although FRR of 2.5 consistently provide the smallest particle size in all conducted experiments, FRR of 1 was considered preferable due to its lower PDI. The decrease in PDI observed with increasing antisolvent (ethanol) amount can be attributed to a decrease in the frequency of particle collisions, subsequently reducing the probability of particle aggregation (Shrimal et al., 2021). According to the screening analysis, the effect of other investigated factors on size and PDI was found to be negligible.

3.1.4. Validation of the design space and selection of the process parameters

Nanoparticles' penetration through the skin structure depends on various factors, especially the nanoparticle size (Baroli, 2010). Specifically for cutaneous mycosis, nanoparticles with size ranging between 100 and 300 nm are preferred because they show suitable penetration into deep skin layers, thereby allowing for a better treatment of dermatophytosis (Garg et al., 2020). Moreover, a reduced PDI (below 0.2) is also preferred since it indicates a greater homogeneity of the nanoformulation (Danaei et al., 2018). Therefore, the design space was used to select the suitable process parameters allowing to obtain KNPs of about 100 nm with a narrow PDI between 0.1 and 0.2. The best process parameters were identified to be a keratin concentration of 1 % w/V, TFR of 14 mL/min, and FRR of 1:1. In order to validate the DoE, the experimental values of size and PDI obtained with the selected process parameters were compared with the theoretical ones (Table 2). The observed agreement between the experimental values and the predicted values indicates that the Box-Behnken design has a high prognostic ability, suggesting its efficacy in predicting the optimal conditions for nanoparticle preparation. Only the KNPs obtained with the selected process parameters were considered for further studies included crosslinking with TA, as well as loading with TCZ.

3.2. Crosslinking

The cross-linking process was carried out to enhance KNPs' physical characteristics and stabilize KNPs' size and PDI after discharging the organic solvent. The cross-linking profile of KNPs was studied based on size and PDI with GA and TA as the conventional and novel crosslinkers, respectively. In Fig. 4, the size and PDI of nanoparticles treated with different amounts of TA for different reaction times, before (Fig. 4 a and b) and after dialysis (Fig. 4 c and d), were compared. In general, the crosslinked nanoparticles showed sizes higher than 200 nm, that are higher than uncrosslinked ones (about 120 nm). Crosslinking involves the formation of covalent bonds between proteins or other molecules, resulting in the creation of larger molecular complexes. When proteins within nanoformulations undergo crosslinking, they can aggregate or form larger structures (Koebe et al., 2012), which may cause an overall increase in the size of the freshly made formulation. Instead, the one-way ANOVA test (*p-value* < 0.05) revealed not significant differences in size and PDI in function of TA amount and crosslinking time.

For all the tested conditions, the nanoparticles size does not change significantly after dialysis, meaning that the crosslinking process with TA is functional to stabilize the nanoformulation (Fig. 4 c and d).

If compared with the crosslinking process using GA with a previously optimized conditions (Aluigi et al., 2018), it can be seen the GA does not increase the size of freshly made nanoformulation as TA, since the GA crosslinked nanoparticles showed a size of about 100 nm (Fig. 4a).

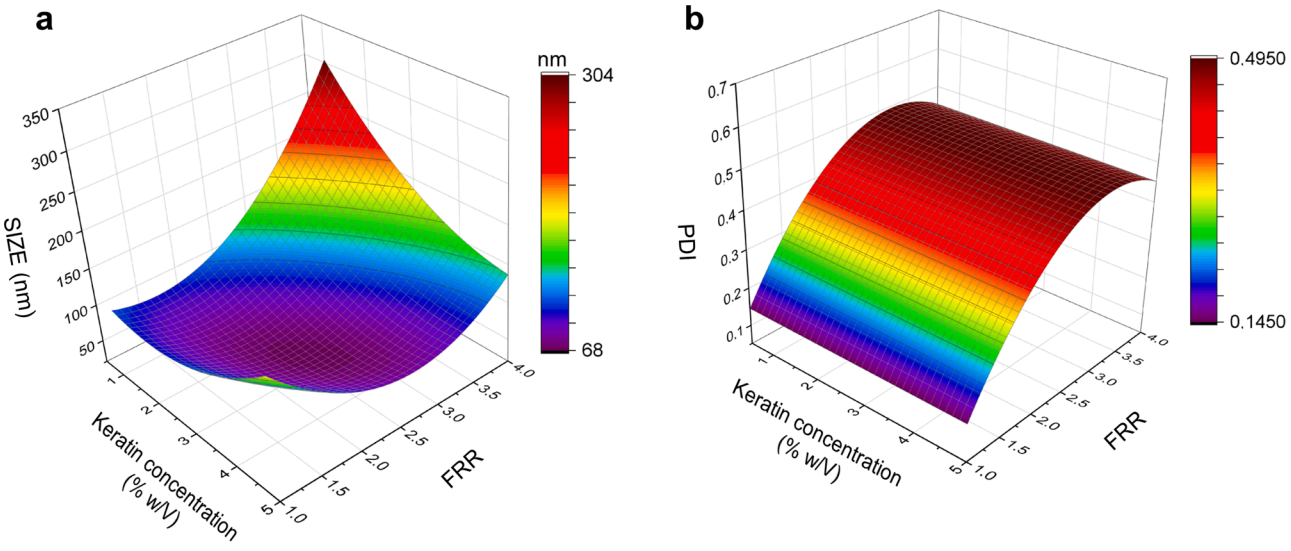

Fig. 3. Design space for size (a) and PDI (b) as function of keratin concentration (X_1) and FRR (X_3) at 22 mL/min of TFR.

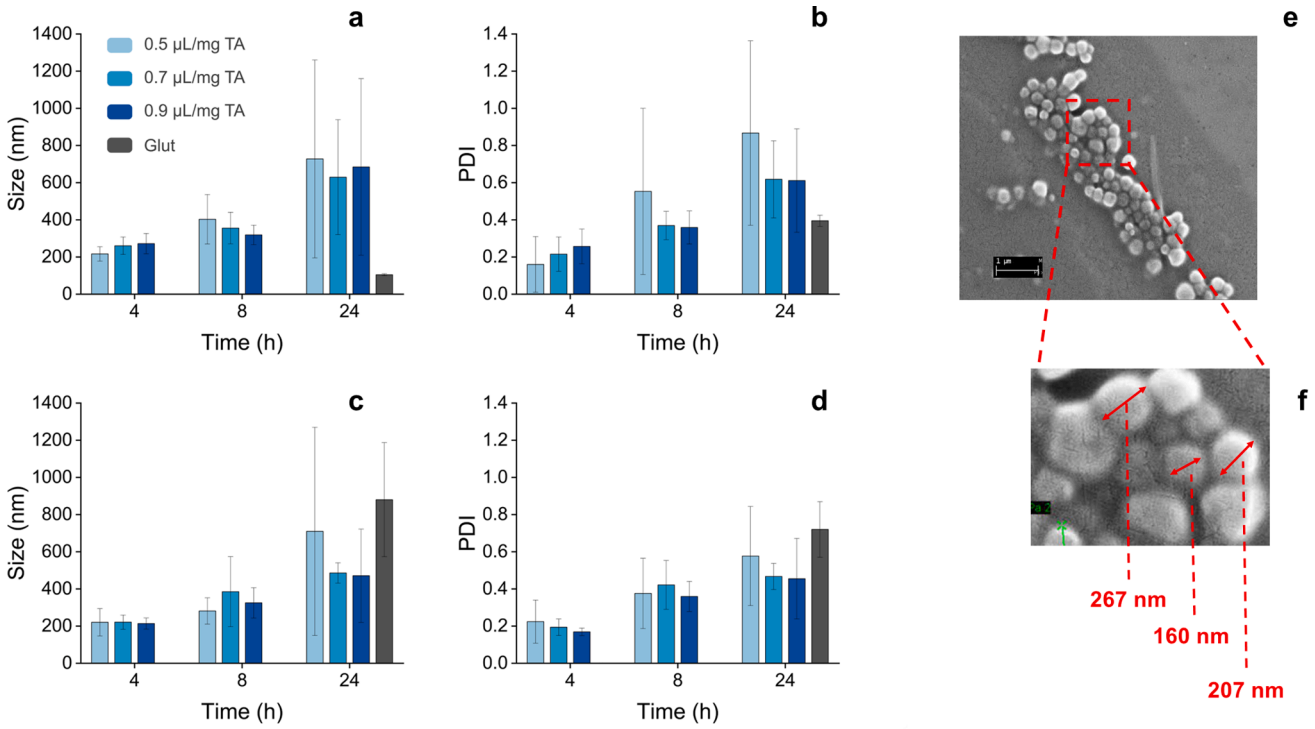

Fig. 4. Effects of TA amount and crosslinking reaction time on size before dialysis (a) and PDI before dialysis (b), size after dialysis (c) and PDI after dialysis (d) – no significant differences was evidenced between the groups by one-way ANOVA; SEM image of nanoparticles crosslinked 0.9 µL/mg keratin of a TA 10 % w/v with 4 h of reacting time and dialyzed (e) and magnification of SEM image with detail about size of dried nanoparticles (f).

However, differently from TA-crosslinked nanoparticles, a significant increase in size of GA-crosslinked nanoparticles can be observed after dialysis (Fig. 4c). Untreated protein nanoparticles tend to swell and undergo size enlargement upon removal of the organic phase. This behaviour can be attributed to the interaction between water molecules from the aqueous phase and the exposed hydrophilic surface of the protein nanoparticles (Qi et al., 2020). The observed significant increase in size following the crosslinking process with GA can be related to incomplete or improper interaction between GA and keratin functional groups. As a consequence, the interaction of water molecules with the untreated keratin surface becomes more prominent after the removal of ethanol, causing further swelling and size augmentation. Based on the experimental results, the selected conditions to stabilize the KNPs were 0.9 µL/mg keratin of a TA 10 % w/v with 4 h of reacting time, since they allow to obtain dialyzed nanoparticles with the smallest size (about 200 nm) and PDI (below 0.2), with a reduced deviation standard which suggests a better homogeneity of the nanoformulations.

In Fig. 4e, the micrograph of the nanoparticles crosslinked using the aforementioned selected conditions and dialyzed are shown. As shown, they appear smooth and homogeneous. Their measured sizes (Fig. 4f) are in agreement with the DLS measurements.

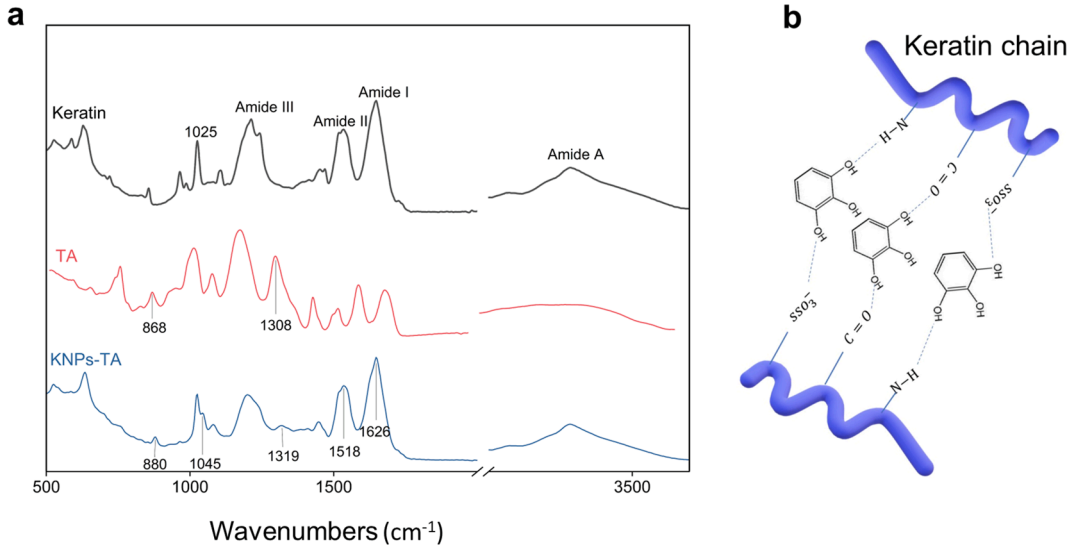

Fig. 5. (a) Physicochemical characterization by FTIR analysis of (a) KNPs- TA, TA, and keratin and demonstrated that interactions between TA and Keratin in crosslinked KNPs were able to slightly change the location of bands, indicating crosslinking reaction. (b) Schematic crosslinking reactions between tannic acid and keratin.

3.3. Fourier-transform infrared spectroscopy (FTIR)

The crosslinking mechanism between TA and proteins that mainly occurs at moderate pH is thought to be non-covalent interactions such as hydrogen bonding, π-bonding, and hydrophobic interactions (Bianco and Savolainen, 1997). To investigate the potential interactions between keratin and TA, the FTIR spectra of both compounds were compared to that of the KNPs synthesized under the optimized crosslinking conditions (Fig. 5a). The analysis revealed distinct absorption peaks characteristics of amides I, II, and III, which are associated with peptide bonds in keratin (Guidotti et al., 2020; Vasconcelos et al., 2008). In the KNPs, the band shapes of amide I (associated with the C = O stretching vibration) and amide II (associated mainly with the N–H bending vibration) are slightly different from those of keratin. The KNPs show a more pronounced shoulder at 1626 cm^{-1} and a less pronounced shoulder at 1518 cm^{-1} compared to keratin. This indicates the involvement of C = O and N–H groups of the peptide bonds in the interaction with TA.

Moreover, a new band appears at 1045 cm^{-1} in the FTIR spectrum of crosslinked KNPs, indicating the potential interaction between the SSO_3^- groups of the sulphonated cysteine (adsorption peak at 1025 cm^{-1}) and TA The adsorption band at 1308 cm^{-1} corresponding to phenol groups of TA shifted to 1319 cm^{-1} in the KNPs, while the band at 868 cm^{-1} associated with the benzene ring shifted to 880 cm^{-1}. Although the crosslinking mechanism between keratin and TA requires further investigation, it is hypothesized that hydrogen bonding occurs between the catechol and pyrogallol groups of TA and C = O and N–H groups of keratin (Fig. 5b).

3.4. Tioconazole loaded keratin nanoparticles (TCZ-KNPs)

Fig. 6a shows the suspensions of keratin nanoparticles loaded with different amounts of tioconazole (TCZ). As can be seen in Fig. 6b, the nanoparticles containing 20 % w/w and 30 % w/w of TCZ display a higher size, while the PDI remains lower than 0.2. Since the KNPs loaded with the highest amount of TCZ (30 % w/w) maintain a dimension lower than 200 nm with a high encapsulation efficiency of 91 ± 2 % and a TCZ loading content of 21.4 ± 0.4 %, this formulation was selected for further characterization.

The TCZ was either adsorbed on the surface of KNPs or entrapped inside them. To determine the drug distribution and its localization in the KNPs, the *in vitro* release of TCZ against ethanol:PBS 30:70 medium was performed. Fig. 7a and c shows the release of tioconazole from the KNPs over time. The release profile was modeled using mono-exponential (Equation (6) and bioexponential (Equation (7) mathematical models:

$$C = C_0 e^{-kt} \quad (6)$$

$$C = ae^{-k_1 t} + be^{-k_2 t} \quad (7)$$

where C_0 and C are the initial drug amount and the drug amount at time t, encapsulated in the nanoparticles, respectively. Drug amount concerning the burst and the sustained release is represented by a and b, respectively. The kinetic constant for burst and sustained release are denoted as k_1 and k_2, respectively. The best fitting was observed by using the bioexponential model since it shows the correlation coefficient R^2 most approaching the unit. The values a and b indicate that there is a burst release involving 61 % of the drug, followed by a sustained release of 37 % of the drug.

The fast release on the initial time, probably corresponds to the drug located on the surface of nanoparticles; while the sustained release corresponds to the amount of drug internalized in the nanoparticles' core as schematized in Fig. 7b. Moreover, the kinetic constant related to the sustained release approaches 0, thereby suggesting that the drug remains entrapped in the nanoparticles. This is desirable behaviour for sustained release since the remaining 30 % of TCZ entrapped in the KNPs can be released upon keratin degradation.

3.5. Cryoprotectant effect of trehalose in the freeze-drying process

Freeze-drying is a commonly used method to stabilize protein nanoparticles in their aqueous solutions, but it can lead to excessive nanoparticle aggregation, hindering their reconstitution in water. To avoid this drawback, sugars have been evaluated as stabilizing agents for proteins during freeze-drying (Imamura et al., 2003). Among them, trehalose showed advantages such as less hygroscopicity, low chemical reactivity, higher glass transition temperature, and absence of internal hydrogen bonds, which allows easier formation of hydrogen bonds with nanoparticles during freeze-drying (ABDELWAHED et al., 2006). The level of stabilization depends on the concentration of cryoprotectants, and adding 5 % (w/v) trehalose was sufficient to prevent nanoparticle aggregation during reconstitution, as seen in Fig. 8a where the size and PDI of the nanoparticle freeze-dried and the reconstitution (5 mg/ml) were compared with the starting formulation.

3.6. Stability of KNPs nanoparticles suspensions

The major obstacle that limits the use of protein nanoparticles is their physical instability (aggregation/particle fusion) and/or the chemical instability (protein degradation by hydrolysis), which are frequent when the aqueous suspensions are stored for an extended period. Therefore, in order to evaluate their stability in liquid form, KNPs suspensions (5 mg/mL) loaded with 30 % of TCZ were stored at 4 °C and their size and PDI were monitored over time. As shown in Fig. 8b, there is no significant change in the size and PDI of KNPs during the 4-week storage at 4 °C, indicating that the suspension remained stable for at least 1 month.

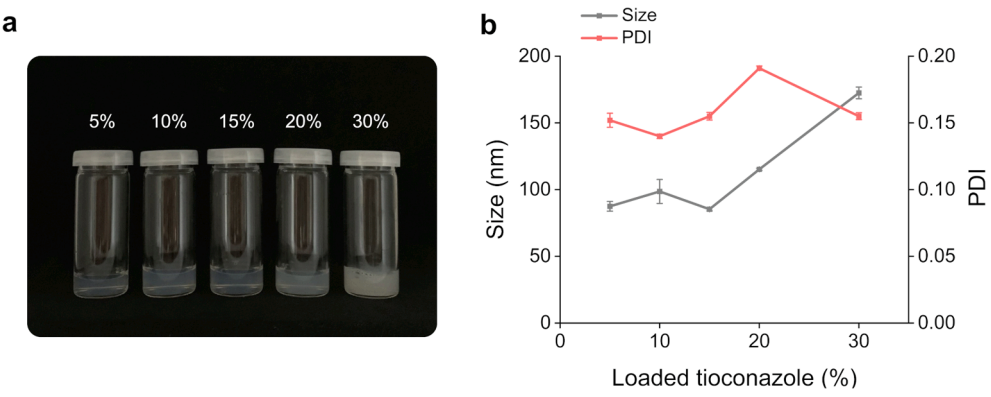

Fig. 6. (a) Visual appearance of the KNPs loaded with different amounts of tioconazole; (b) Size and PDI as function of the amount of loaded TCZ.

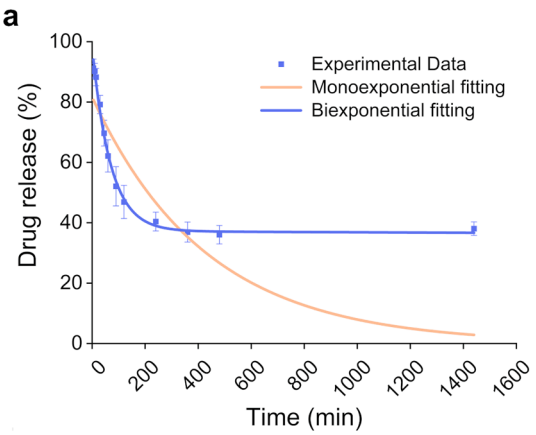

Monoexponential model	
K (Min^{-1})	0.0023±0.0007
R^2	0.589
Biexponential model	
a (%)	61±1
b (%)	37±1
K_1 (Min^{-1})	0.0014±0.0007
K_2 (Min^{-1})	0.00001±0.00001
R^2	0.995

Fig. 7. (a) Drug release profile of tioconazole, (b) schematic representation of the TCZ distribution in the KNPs, and (c) curve fitting with monoexponential and biexponential mathematical models.

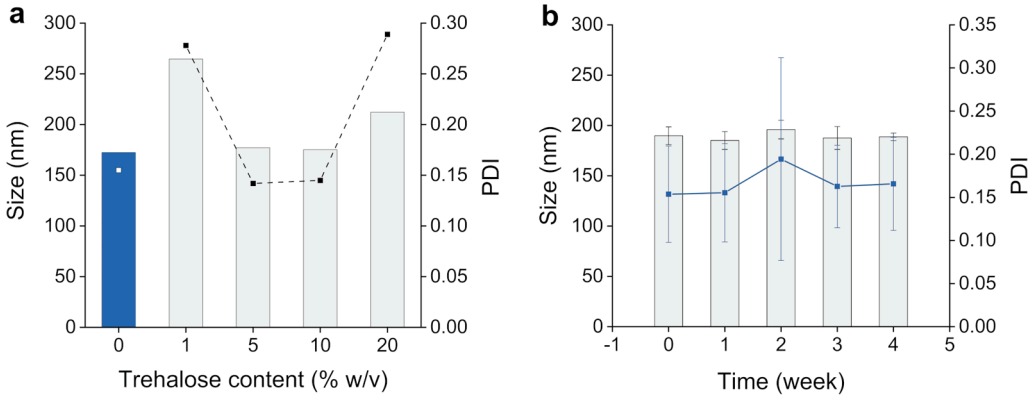

Fig. 8. (a) Size and PDI of reconstituted TCZ-KNPs as function of trehalose content; (b) Size and PDI of TCZ-KNPs suspended in water (5 mg/mL), as function of time.

3.7. Cytocompatibility and microbiological studies

Cytotoxicity of the liposomes toward normal HaCaT cells was evaluated by both SRB and WST-8 assays. As observed in Figure S2, the KNPs did not show any cytotoxic effects within the range of concentrations tested, up to 1 mg/mL as compared to untreated control cells. No significant differences in cell viability were evidenced by WST-8 and SRB assays after KNP administration to HaCaT cells.

As for the tests carried out with the microdilution method, both TCZ and TCZ-KNPs cause partial growth inhibition at higher dilutions compared to the control wells with some variations in repeats and strains. The minimum inhibitory concentration (MIC) of *M. canis* was observed at dilution 7 for TCZ-KNPs (dilution 8 for strain 59) and at dilution 4 for TCZ. On the other hand, KNPs alone cause growth inhibition only at the higher concentration.

The Minimum lethal concentration (MLC) on agar plates was observed at dilution 4 for TCZ-KNPs and at dilution 2 for TCZ. No lethal concentration was observed with KNPs alone for strains 139 and 80, while concentration 1 showed a lethal effect on strain 59. The MIC and MLC values for the three strains tested are reported in Table 4.

The results obtained showed that TCZ-KNPs have been able to give 100 % growth inhibition at a a concentration of TCZ three-fold lower than that required for free TCZ.

The MLC of the TCZ-KNPs contained the same concentration of TCZ corresponding to the MIC for TCZ alone. Strain 59 seemed to be more sensitive to the presence of keratin, so much so that for this strain the MIC of TCZ-KNPs was lower by one dilution than those of the other strains, and KNPs alone at the highest concentration tested showed not only an inhibitory effect but also a lethal effect.

Table 4
MIC and MLC of the products tested on three strains of M. canis.

Product	**TCZ-KNPs**		**TCZ**		**KNPs**	
Tested Strain	MIC mg/mL	MLC mg/mL	MIC mg/mL	MLC mg/mL	MIC mg/mL	MLC mg/mL
139	0.0156 *	0.125^	0.034	0.136	1	nd
80	0.0156 *	0.125^	0.034	0.136	1	nd
59	0.0078 §	0.125^	0.034	0.136	1	1

* content of TCZ = 0.0042 mg/ml; § content of TCZ = 0.0021 mg/mL;^content on TCZ = 0.034 mg/mL.

Concerning the diffusion tests on agar, after 4 days of incubation, distinct inhibition halos were observed around the deposited drops of TCZ-KNPs. In contrast, halos were also present for TCZ, but they were only partial, with numerous points of fungal growth within the halos. No inhibition effect was observed around the deposited drops of KNPs alone. At the final reading after 11 days, the inhibition halos in the TCZ plates had almost completely disappeared, whereas the TCZ-KNPs plates still shows a persistent inhibitory effect around the deposition point (Fig. 9).

Therefore, TCN-KNPs seem to determine a more persistent inhibitory effect over time. This could be due to the sustained release of TCZ, observed when it is loaded on keratin nanoparticles.

Previous tests (data not shown) using concentration 1 of the dilution tests, had not shown any inhibitory effect for TCZ alone, but an effect similar to that described in this test for TCZ-KNPs was present.

The inhibition of *M. canis* grown on hair *in vitro* was also evaluated. After 12 days, no mycelium growth was observed in the wells containing

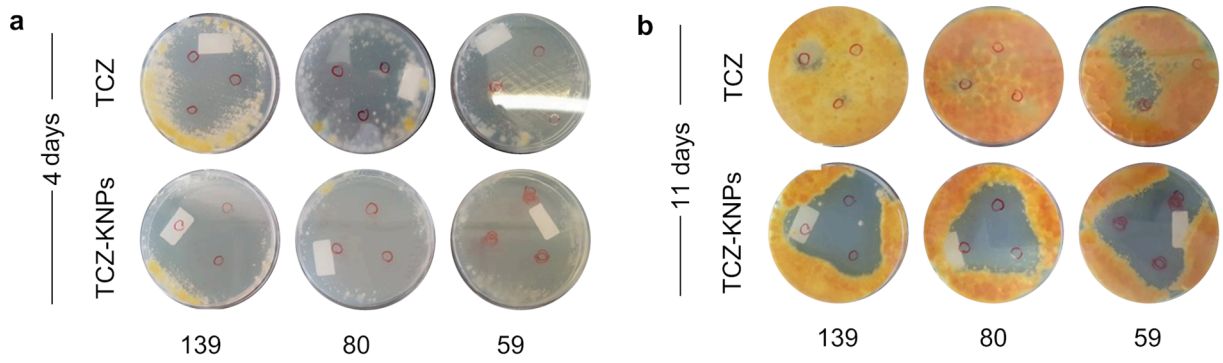

Fig. 9. Inhibition halos around the deposit site of TCZ and TCZ-KNPs of the three strains of M. canis were tested, (a) after 4 and (b) 11 days.

the infected hair in all the tested dilution (from 1 to 5 of Table 2) of both KNPs and TCZ-KNPs, while evident growth of mycelium is observed in the control wells. The MIC was established at < 0.0625 mg/ml for TCN-KNPs and at < 0.017 mg/ml for tioconazole against strains 80 and 59. Hair from strain 139 cultures were found to be contaminated by Penicillium sp., therefore no longer considered. The hair transferred on SAB-CAF plates after different times of contact, showed no or slow growth at the highest concentrations when contact time increased. Also, in this case, the TCZ-KNPs maintained a growth-inhibiting effect on agar longer than free TCZ. Nevertheless, after 20 days it has been observed a mycocidal effect of the TCZ-KNPs at the concentration 1 of Table 2 and after 48 h, and 120 h of their contact with hair; while, after 12 days/ contact the mycocidal effect was present also at dilutions 3 (Fig. 10).

It is worth considering that the *in vitro* grown on hair does not completely reproduce the conditions that occur in the parasitic phase, where typical more resistant arthrospores are also produced. However, this approach allows obtaining hairs with internal hyphae (perforating organs) protected by the hair itself, which can be used for contact simulations with the tested products. As a result, the concentration required to achieve a mycocidal effect is higher compared to the micro method. This is likely due to the fact that at lower concentrations and contact times, the protected hyphae inside the hairs may still exhibit inhibition but are not completely inactivated by the tested products.

4. Conclusion

In conclusion, this study successfully developed a tunable, reproducible, and scalable manufacturing process for keratin nanoparticles by means of microfludic-assisted desolvation process. The design space correlating nanoparticles properties with manufacturing processes and defined through a BBD-DoE approach, proved to be effective, with the calculated values closely matching the experimental results for size and polydispersity index.

Additionally, the use of tannic acid as a cross-linker demonstrated superior effectiveness compared to glutaraldehyde as the conventional crosslinker. Regarding storage and administration, freeze-drying of the KNPs with 5 % trehalose as a stabilizing agent prevented nanoparticle aggregation, allowing for easy reconstitution. The developed tioconazole-loaded keratin nanoparticles exhibited cytocompatibility, making them a promising drug delivery system for the treatment of mycosis. In the future work, besides the study of pilot-scale upscaling of the manufacturing process of TCZ-KNPs, further biological validations on *ex-vivo* human skin, as well as *in-vivo* evaluations will be carried out in order to fully explore the therapeutic potential of this new formulation.

ASSOCIATED CONTENT

1. Experimental design and DLS experiment
2. Cell viability test

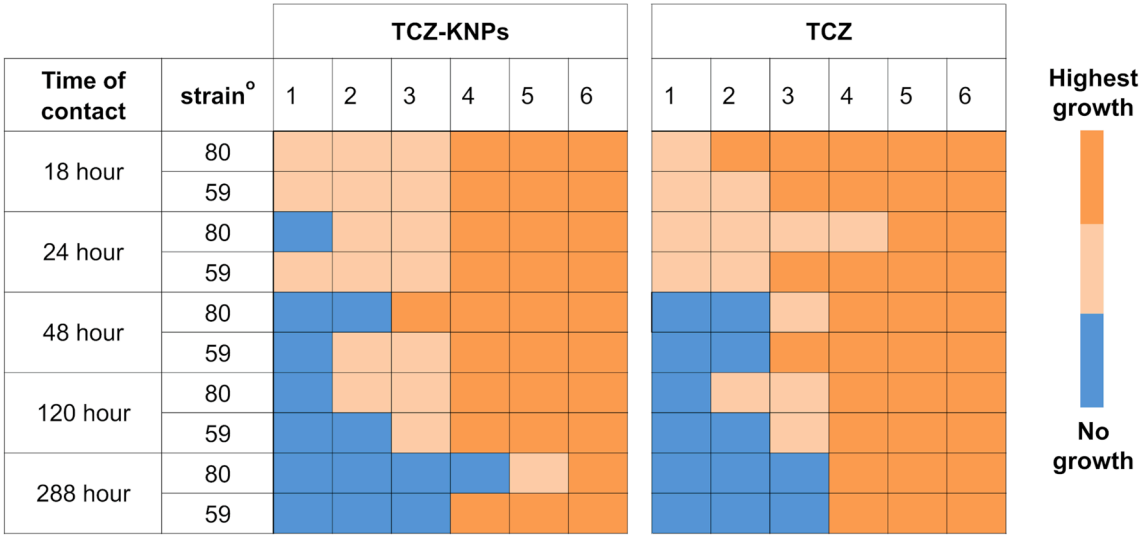

Fig. 10. Scheme of the presence of *M. canis* mycelial growth after 20 days of the inoculum in SAB-CAF agar of *in vitro* infected hair after different times of contact with the tested concentration of TCZ or TCZ-KNPs. Legend: blu = no growth, pink = slow growth, orange = full growth. The tested concentrations were (in order 1–5): 1; 0.5; 0.25; 0.125, 0.0625 mg/mL for TCZ-KNPs, and 0.272; 0.136; 0.068; 0.035; 0.017 mg/mL for free TCZ. Column 6 is relative to the control, with only culture medium. (For interpretation of the references to color in this figure legend, the reader is referred to the web version of this article.)

3. *In vitro* hair perforation by *M. canis*

CRediT authorship contribution statement

Shiva Khorshid: Methodology, Visualization, Data curation, Investigation, Writing – original draft. **Rosita Goffi:** Methodology, Visualization. **Giorgia Maurizii:** Methodology, Visualization. **Serena Benedetti:** Methodology, Writing – original draft. **Giovanna Sotgiu:** Conceptualization, Validation, Visualization. **Roberto Zamboni:** Conceptualization, Validation, Visualization. **Sara Buoso:** Methodology. **Roberta Galuppi:** Methodology, Data curation, Investigation, Writing – original draft. **Talita Bordoni:** Methodology. **Mattia Tiboni:** Writing – review & editing. **Annalisa Aluigi:** Conceptualization, Supervision, Data curation, Formal analysis, Writing – original draft, Writing – review & editing. **Luca Casettari:** Supervision, Writing – review & editing, Resources.

Declaration of Competing Interest

The authors declare that they have no known competing financial interests or personal relationships that could have appeared to influence the work reported in this paper.

Data availability

Data will be made available on request.

Acknowledgment

The work was carried out with co-financing of the MICOSKER- POR-FESR EMILIA ROMAGNA 2014-2020 (PG/2021/683277 29/07/2021) and of the European Union – Next Generation EU - PNRR MUR project ECS_00000041-VITALITY".

The authors acknowledge ITIS E. Mattei (Urbino, PU, Italy) for the utilization of the FTIR instrument.

The authors also acknowledge Michele Casappa and Franco Corticelli of the National Research Council of Italy for the preliminary test with tioconazole loaded keratin nanoparticles and for the SEM analysis, respectively.

Appendix A. Supplementary data

Supplementary data to this article can be found online at https://doi.org/10.1016/j.ijpharm.2023.123489.

References

Abdelwahed, W., Degobert, G., Stainmesse, S., Fessi, H., 2006. Freeze-drying of nanoparticles: Formulation, process and storage considerations☆. Adv. Drug Deliv. Rev. 58, 1688–1713. https://doi.org/10.1016/j.addr.2006.09.017.

Ahmadian, Z., Correia, A., Hasany, M., Figueiredo, P., Dobakhti, F., Eskandari, M.R., Hosseini, S.H., Abiri, R., Khorshid, S., Hirvonen, J., Santos, H.A., Shahbazi, M.A., 2021. A hydrogen-bonded extracellular matrix-mimicking bactericidal hydrogel with radical scavenging and hemostatic function for pH-responsive wound healing acceleration. Adv. Healthc. Mater. 10 https://doi.org/10.1002/adhm.202001122.

Aluigi, A., Sotgiu, G., Ferroni, C., Duchi, S., Lucarelli, E., Martini, C., Posati, T., Guerrini, A., Ballestri, M., Corticelli, F., Varchi, G., 2016. Chlorin e6 keratin nanoparticles for photodynamic anticancer therapy. RSC Adv. 6, 33910–33918. https://doi.org/10.1039/C6RA04208B.

Aluigi, A., Ballestri, M., Guerrini, A., Sotgiu, G., Ferroni, C., Corticelli, F., Gariboldi, M.B., Monti, E., Varchi, G., 2018. Organic solvent-free preparation of keratin nanoparticles as doxorubicin carriers for antitumour activity. Mater. Sci. Eng. C 90, 476–484. https://doi.org/10.1016/j.msec.2018.04.088.

Amaral, A.C., Felipe, M.S.S., 2013. Nanobiotechnology: An efficient approach to drug delivery of unstable biomolecules. Curr. Protein Pept. Sci. 14, 588–594. https://doi.org/10.2174/1389203711209070632.

Baroli, B., 2010. Penetration of nanoparticles and nanomaterials in the skin: Fiction or reality? J. Pharm. Sci. 99, 21–50. https://doi.org/10.1002/jps.21817.

Bianco, M.A., Savolainen, H., 1997. Phenolic acids as indicators of wood tannins. Sci. Total Environ. 203, 79–82. https://doi.org/10.1016/S0048-9697(97)00135-6.

Chun, H.J., Park, C.H., Kwon, I.K., Khang, G. (Eds.), 2018. Cutting-edge enabling technologies for regenerative medicine. Springer, Singapore. https://doi.org/10.1007/978-981-13-0950-2.

Clissold, S.P., Heel, R.C., 1986. Tioconazole. Drugs 31, 29–51. https://doi.org/10.2165/00003495-198631010-00003.

Costa, A.F., Luís, S., Noro, J., Silva, S., Silva, C., Ribeiro, A., 2022. Therapeutic textiles functionalized with keratin-based particles encapsulating terbinafine for the treatment of onychomycosis. Int. J. Mol. Sci. 23, 13999. https://doi.org/10.3390/ijms232213999.

Danaei, M., Dehghankhold, M., Ataei, S., Hasanzadeh Davarani, F., Javanmard, R., Dokhani, A., Khorasani, S., Mozafari, M.R., 2018. Impact of particle size and polydispersity index on the clinical applications of lipidic nanocarrier systems. Pharmaceutics. https://doi.org/10.3390/pharmaceutics10020057.

Dube, A., Reynolds, J.L., Law, W.-C., Maponga, C.C., Prasad, P.N., Morse, G.D., 2014. Multimodal nanoparticles that provide immunomodulation and intracellular drug delivery for infectious diseases. Nanomedicine 10, 831–838. https://doi.org/10.1016/j.nano.2013.11.012.

Forigua, A., Kirsch, R.L., Willerth, S.M., Elvira, K.S., 2021. Recent advances in the design of microfluidic technologies for the manufacture of drug releasing particles. J. Control. Release 333, 258–268. https://doi.org/10.1016/j.jconrel.2021.03.019.

Galuppi, R., Gambarara, A., Bonoli, C., Ostanello, F., Tampieri, M.P., 2010. Antimycotic effectiveness against dermatophytes: Comparison of two in vitro tests. Vet. Res. Commun. 34, 57–61. https://doi.org/10.1007/s11259-010-9386-1.

Garg, A., Sharma, G.S., Goyal, A.K., Ghosh, G., Si, S.C., Rath, G., 2020. Recent advances in topical carriers of anti-fungal agents. Heliyon 6, e04663. https://doi.org/10.1016/j.heliyon.2020.e04663.

Giannelli, M., Guerrini, A., Ballestri, M., Aluigi, A., Zamboni, R., Sotgiu, G., Posati, T., 2022. Bioactive keratin and fibroin nanoparticles: An Overview of their preparation strategies. Nanomaterials 12, 1406. https://doi.org/10.3390/nano12091406.

Guidotti, G., Soccio, M., Posati, T., Sotgiu, G., Tiboni, M., Barbalinardo, M., Valle, F., Casettari, L., Zamboni, R., Lotti, N., Aluigi, A., 2020. Regenerated wool keratin-polybutylene succinate nanofibrous mats for drug delivery and cells culture. Polym. Degrad. Stab. 179, 109272. https://doi.org/10.1016/j.polymdegradstab.2020.109272.

Gülçin, İ., Huyut, Z., Elmastaş, M., Aboul-Enein, H.Y., 2010. Radical scavenging and antioxidant activity of tannic acid. Arab. J. Chem. 3, 43–53. https://doi.org/10.1016/j.arabjc.2009.12.008.

Hashiba, A., Toyooka, M., Sato, Y., Maeki, M., Tokeshi, M., Harashima, H., 2020. The use of design of experiments with multiple responses to determine optimal formulations for in vivo hepatic mRNA delivery. J. Control. Release 327, 467–476. https://doi.org/10.1016/j.jconrel.2020.08.031.

Havlickova, B., Czaika, V.A., Friedrich, M., 2008. Epidemiological trends in skin mycoses worldwide. Mycoses 51, 2–15. https://doi.org/10.1111/j.1439-0507.2008.01606.x.

Imamura, K., Ogawa, T., Sakiyama, T., Nakanishi, K., 2003. Effects of types of sugar on the stabilization of protein in the dried state. J. Pharm. Sci. 92, 266–274. https://doi.org/10.1002/jps.10305.

Khorshid, S., Montanari, M., Benedetti, S., Moroni, S., Aluigi, A., Canonico, B., Papa, S., Tiboni, M., Casettari, L., 2022. A microfluidic approach to fabricate sucrose decorated liposomes with increased uptake in breast cancer cells. Eur. J. Pharm. Biopharm. 178, 53–64. https://doi.org/10.1016/j.ejpb.2022.07.015.

Koebe, M., Drechsler, M., Weber, J., Yuan, J., 2012. Crosslinked poly(ionic liquid) nanoparticles: Inner structure, size, and morphology. Macromol Rapid Commun 33, 646–651. https://doi.org/10.1002/marc.201100836.

Kurtzman, C.P., Fell, J.W., Boekhout, T., Robert, V., 2011. Methods for isolation, phenotypic characterization and maintenance of yeasts. In: The Yeasts. Elsevier, pp. 87–110. https://doi.org/10.1016/B978-0-444-52149-1.00007-0.

Li, N., Yang, X., Liu, W., Xi, G., Wang, M., Liang, B., Ma, Z., Feng, Y., Chen, H., Shi, C., 2018. Tannic acid cross-linked polysaccharide-based multifunctional hemostatic microparticles for the regulation of rapid wound healing. Macromol. Biosci. 18, 1800209. https://doi.org/10.1002/mabi.201800209.

Luo, G., Du, L., Wang, Y., Lu, Y., Xu, J., 2011. Controllable preparation of particles with microfluidics. Particuology 9, 545–558. https://doi.org/10.1016/j.partic.2011.06.004.

Ma, Z., Li, B., Peng, J., Gao, D., 2022. Recent development of drug delivery systems through microfluidics: From synthesis to evaluation. Pharmaceutics 14, 434. https://doi.org/10.3390/pharmaceutics14020434.

Mercer, D.K., Stewart, C.S., 2019. Keratin hydrolysis by dermatophytes. Med. Mycol. 57, 13–22. https://doi.org/10.1093/mmy/myx160.

MONTGOMERY, D.C., 2012. Design and Analysis of Experiments, 8th ed. John Wiley & Sons.

Ninan, N., Forget, A., Shastri, V.P., Voelcker, N.H., Blencowe, A., 2016. Antibacterial and anti-inflammatory ph-responsive tannic acid-carboxylated agarose composite hydrogels for wound healing. ACS Appl. Mater. Interfaces 8, 28511–28521. https://doi.org/10.1021/acsami.6b10491.

Qi, H., Yang, L., Shan, P., Zhu, S., Ding, H., Xue, S., Wang, Y., Yuan, X., Li, P., 2020. The stability maintenance of protein drugs in organic coatings based on nanogels. Pharmaceutics 12. https://doi.org/10.3390/pharmaceutics12020115.

Rebollo, R., Oyoun, F., Corvis, Y., El-Hammadi, M.M., Saubamea, B., Andrieux, K., Mignet, N., Alhareth, K., 2022. Microfluidic manufacturing of liposomes: Development and optimization by design of experiment and machine learning. ACS Appl. Mater. Interfaces 14, 39736–39745. https://doi.org/10.1021/acsami.2c06627.

Rocha, K.A.D., Krawczyk-Santos, A.P., Andrade, L.M., de Souza, L.C., Marreto, R.N., Gratieri, T., Taveira, S.F., 2017. Voriconazole-loaded nanostructured lipid carriers (NLC) for drug delivery in deeper regions of the nail plate. Int. J. Pharm. 531, 292–298. https://doi.org/10.1016/j.ijpharm.2017.08.115.

Sarker, P., Nalband, D.M., Freytes, D.O., Rojas, O.J., Khan, S.A., 2022. High-axial-aspect tannic acid microparticles facilitate gelation and injectability of collagen-based hydrogels. Biomacromolecules 23, 4696–4708. https://doi.org/10.1021/acs.biomac.2c00916.

Shrimal, P., Jadeja, G., Patel, S., 2021. Microfluidics nanoprecipitation of telmisartan nanoparticles: Effect of process and formulation parameters. Chem. Pap. 75, 205–214. https://doi.org/10.1007/s11696-020-01289-w.

Singh, S.N., Tripathi, R.D., et al., 2007. Environmental bioremediation technologies. Springer Berlin Heidelberg, Berlin, Heidelberg. https://doi.org/10.1007/978-3-540-34793-4.

Souza, A.C.O., Amaral, A.C., 2017. Antifungal therapy for systemic mycosis and the nanobiotechnology era: Improving efficacy, Biodistribution and toxicity. Front Microbiol 8. https://doi.org/10.3389/fmicb.2017.00336.

Tao, H., Wu, T., Kheiri, S., Aldeghi, M., Aspuru-Guzik, A., Kumacheva, E., 2021. Self-driving platform for metal nanoparticle synthesis: combining microfluidics and machine learning. Adv. Funct. Mater. 31 https://doi.org/10.1002/adfm.202106725.

Tiboni, M., Benedetti, S., Skouras, A., Curzi, G., Perinelli, D.R., Palmieri, G.F., Casettari, L., 2020. 3D-printed microfluidic chip for the preparation of glycyrrhetinic acid-loaded ethanolic liposomes. Int. J. Pharm. 584, 119436. https://doi.org/10.1016/j.ijpharm.2020.119436.

Tiboni, M., Tiboni, M., Pierro, A., Del Papa, M., Sparaventi, S., Cespi, M., Casettari, L., 2021. Microfluidics for nanomedicines manufacturing: An affordable and low-cost 3D printing approach. Int. J. Pharm. 599, 120464. https://doi.org/10.1016/j.ijpharm.2021.120464.

Toms, D., Deardon, R., Ungrin, M., 2017. Climbing the mountain: experimental design for the efficient optimization of stem cell bioprocessing. J Biol Eng 11, 35. https://doi.org/10.1186/s13036-017-0078-z.

Valencia, P.M., Farokhzad, O.C., Karnik, R., Langer, R., 2012. Microfluidic technologies for accelerating the clinical translation of nanoparticles. Nat. Nanotechnol. 7, 623–629. https://doi.org/10.1038/nnano.2012.168.

Vasconcelos, A., Freddi, G., Cavaco-Paulo, A., 2008. Biodegradable materials based on silk fibroin and keratin. Biomacromolecules 9, 1299–1305. https://doi.org/10.1021/bm7012789.

Whiteley, Z., Ho, H.M.K., Gan, Y.X., Panariello, L., Gkogkos, G., Gavriilidis, A., Craig, D. Q.M., 2021. Microfluidic synthesis of protein-loaded nanogels in a coaxial flow reactor using a design of experiments approach. Nanoscale Adv 3, 2039–2055. https://doi.org/10.1039/d0na01051k.

Zhang, L., Chen, Q., Ma, Y., Sun, J., 2020. Microfluidic methods for fabrication and engineering of nanoparticle drug delivery systems. ACS Appl Bio Mater 3, 107–120. https://doi.org/10.1021/acsabm.9b00853.